AIP | Review of Scientific Instruments

Infrared imaging video bolometer for the large helical device

B. J. Peterson, M. Osakabe, M. Shoji, and N. Ashikawa

Citation: Rev. Sci. Instrum. **72**, 923 (2001); doi: 10.1063/1.1319597

View online: http://dx.doi.org/10.1063/1.1319597

View Table of Contents: http://rsi.aip.org/resource/1/RSINAK/v72/i1

Published by the American Institute of Physics.

Infrared imaging video bolometer for the large helical device

B. J. Peterson,[a] M. Osakabe, and M. Shoji
National Institute for Fusion Science, Toki-shi, 509-5292, Japan

N. Ashikawa
Graduate University for Advanced Studies, Toki-shi 509-5292, Japan

(Presented on 21 June 2000)

A new type of infrared imaging bolometer, known as the infrared imaging video bolometer (IRVB) has been under development at the National Institute of Fusion Science (NIFS) over the last year. A prototype of this diagnostic has been designed and constructed at NIFS and installed on the large helical device (LHD) and successfully operated. This diagnostic utilizes a $66\times90\times0.001$ mm gold foil mounted in a frame to detect the radiation and neutrals from the plasma which are incident on the foil through a 1 cm diameter pinhole. The resulting temperature distribution on the foil is measured using an AGEMA THV 900 LW infrared camera having 136×272 pixels with a frame rate of 15 Hz and a nominal sensitivity of 80 mK. An image of the foil and surrounding frame consisting of 120×160 pixels is resampled down to 12×16 pixels using a linear interpolation scheme. Using a numerical technique the spatial and temporal derivatives of the temperature distribution on the foil are calculated and the incident power density on the foil is determined using a calibration of the foil obtained by means of a HeNe laser. The resulting 10×14 pixel view of the plasma radiation at a 15 Hz frame rate has a noise equivalent power density of 0.5 mW/cm^2. The IRVB was mounted on a LHD tangential port for the 1999 campaign. An image of the plasma radiation during a discharge using the inboard vacuum vessel wall as a limiter shows radiation localized near the limiting surface.
[DOI: 10.1063/1.1319597]

I. INTRODUCTION

Broadband radiated power measurements on fusion devices are commonly carried out using metal-foil thermoresistor bolometer elements arranged in either a single detector arrangement for 2π total radiated power measurement or in single or multiple one-dimensional arrays for one- or two-dimensional tomography of the plasma radiation.[1–3] These conventional detectors have the disadvantage of requiring up to five wires per channel, which must be brought through the vacuum interface to the bridge electronics circuit, making them susceptible to vacuum leaks and electromagnetic noise. In order to avoid these problems, bolometers using infrared detectors to measure the temperature of a foil exposed to the plasma were first applied 20 years ago in a single detector/single foil scheme.[4,5] The development of infrared (IR) cameras led to the proposal of their use for the purposes of fusion plasma bolometry.[6] The suggestion of a method utilizing the IR camera's two-dimensional image to provide a two-dimensional bolometer diagnostic involved a matrix of raised absorbers which was simultaneously exposed to the plasma through a pinhole and viewed by the IR camera through a series of IR mirrors and an IR vacuum window.[7] This evolved into a two-dimensional matrix of foil detectors created by sandwiching a thin foil between two identical copper masks known as the segmented mask infrared imaging bolometer (SIB).[8] On one side the foil matrix is exposed to the plasma radiation through a pinhole and on the other side the resulting temperature rise of the foil pixels is measured by an IR camera through an IR vacuum window. The copper mask serves to define the foil pixel size and arrangement and cool and thermally isolate the foil pixels from each other. This concept was first tested on the compact helical system[9] and another version has been installed and operated on the large helical device (LHD).[10] A variation of this diagnostic known as the infrared imaging video bolometer (IRVB), which replaces the foil mask assembly with a single large foil mounted in a frame was recently proposed.[11] This concept relies on a numerical method to solve for the diffusive contribution to the change in the foil temperatures instead of relying on the mask to thermally isolate the pixels. Compared to the SIB, this results in a five-fold increase in the sensitivity of the diagnostic with improved spatial resolution and experimental flexibility at the cost of the loss of support from the mask. In this article we describe the first realization of an IRVB in the design, construction, installation and operation of this diagnostic on the LHD during the 1999 experimental campaign.

II. LHD AND ITS DEMANDS FOR DIAGNOSTICS

LHD is the world's largest helical magnetic plasma confinement device with a major radius of 3.9 m and an average minor radius of 0.6 m. Utilizing superconducting helical and poloidal field coils, the LHD is designed to explore new steady-state operation regimes. The maximum magnetic field at the magnetic axis was 2.9 T during the 1999 campaign. The input power was limited to approximately 5 MW of

[a]Electronic mail: peterson@LHD.nifs.ac.jp

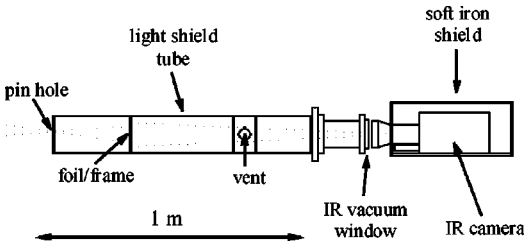

FIG. 1. CAD drawing of side view of the LHD IRVB.

combined neutral beam injection (NBI), electron cyclotron resonance heating (ECRH), and ion cyclotron resonance heating with total radiated power up to 2 MW.

Because of the nonaxisymmetric nature of its helical magnetic field, two-dimensional diagnostics with capabilities for three-dimensional measurements through tomography are needed to interpret the physics of the LHD. Therefore, the development of imaging bolometers is very appropriate for the LHD. Additionally, since one of the main objectives of the LHD experimental program is to explore the physics of steady-state plasmas, steady-state diagnostics including bolometers are needed. In this respect, infrared imaging bolometers have a great advantage over conventional thermoresistive bolometers. Thermorsistive bolometers are not well suited to long term measurement due to signal drift from the detector thermal drift and electronic drift. While thermal drift in thermoresistive bolometers can be reduced by using a reference resistive element to balance the sensing resistor, this balance is not perfect and this results in a long term drift of the signal. Infrared imaging bolometers are not susceptible to electronic drift and the thermal drift of the foil and frame or mask is measured and compensated for in the data analysis. Therefore, IR imaging bolometers are well suited to steady-state diagnosis.

III. THE DESIGN OF THE IRVB FOR THE LHD

The design of the LHD IRVB is shown in a computer aided design (CAD) drawing in Fig. 1. The IRVB consists of a pinhole plate, light shielding tube, foil-in frame, IR vacuum window, soft iron shield and IR camera which are detailed later. The pinhole plate is made of 5-mm-thick stainless steel and the circular pinhole is beveled to a minimum diameter of 1 cm. The shielding tube is made of 1-mm-thick aluminum and has a light tight vent located near the IR window to relieve air pressure differences between the inside and outside of the tube during vacuum pump down. The vent hole is covered with two layers of electroformed grid which are used to prevent microwaves from entering the tube and heating the foil or damaging the IR window.[12] While it is possible to install shielding grids over the pinhole also, we chose not to do so at this time as ECRH using high power microwaves (84 and 168 GHz, 0.4–1 MW) is typically used on the LHD only to produce a seed plasma for NBI and the grids would decrease the signals level by 20%. The inside surfaces of the pinhole plate and light shielding tube are blackened with graphite spray to prevent reflection of infrared light.

The foil-in-frame assembly is shown in Fig. 2. The

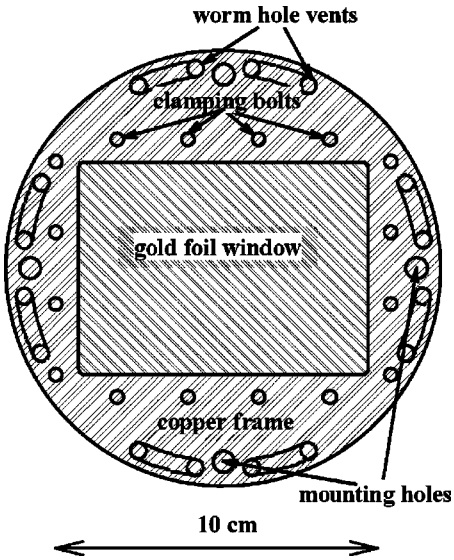

FIG. 2. CAD drawing of frame for foil of the LHD IRVB.

frame is made from two plates of 2-mm-thick oxygen-free copper. A $100\times100\times0.001$ mm gold foil is sandwiched between the frames exposed on either side by holes in the frame pieces having the dimensions 66×90 mm. Bolts are used to tighten the frames together around the edge of the foil in order to assure good contact between the gold foil and the frame. Care must be taken to support the foil during assembly in the frame until the bolts are tightened. After assembly the foil and frame are blackened on the IR camera side with graphite spray in order to increase the IR emissivity. Using a groove and offset hole pattern cut into the frames, eight light-tight ''wormhole'' vents are formed around the periphery of the frame. These vents are intended to relieve any pressure differences which may arise between the two sides of the foil during vacuum pump down and up to air vents.

The vacuum IR window is made from zinc selinide mounted in a 100 mm inner diameter, 150 mm outer diameter vacuum flange. The window is coated for a flat IR transmission of greater than 95% over the wavelength range 3–12 μm. The IR camera is an AGEMA THV 900 LW model with a scanning HgCdTe detector and a Stirling cooler. The wavelength range of the camera is 8–12 μm, the frame rate is 15 Hz for 136×272 pixels, and the nominal sensitivity is 80 mK at 30 °C. The camera is equipped with a telephoto lens having a field of view of $5\times10°$. A fiber optic link is used to remotely operate the IR camera from the control room. Data from the camera can be acquired in 12-bit format and stored in a hard disk. A 6-mm-thick soft iron box is used to shield the camera from magnetic fields. At a maximum axis magnetic field of 2.9 T the magnetic field at the IR camera location is 126 G. Problems with operating this camera at an upper port due to strong magnetic fields have been reported elsewhere.[10] However, we have not experienced any problems with the camera at the tangential port location of the IRVB due to the relatively small value of the stray magnetic field at that location (an order of magnitude smaller than that at the upper port).

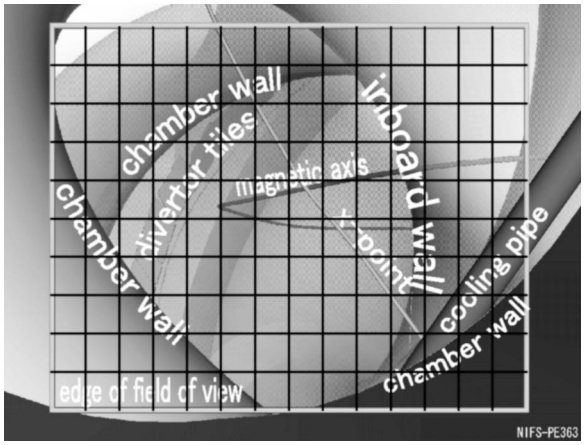

FIG. 3. CAD drawing of the field of view of the LHD IRVB from a tangential port.

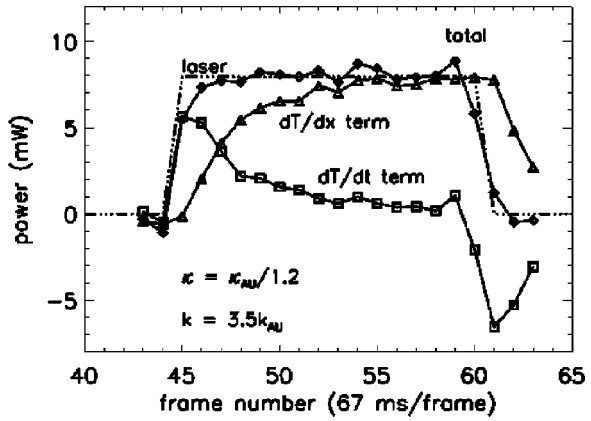

FIG. 4. Time evolution of laser power (broken line) and measured laser power (diamonds—total, traiangles—time derivative term, squares—spatial derivative term) for $\kappa=\kappa_{AU}/1.2$ and $k=3.5k_{AU}$.

The IRVB is installed at a tangential port located 21 cm below the midplane. A CAD drawing of the view of the bolometer is shown in Fig. 3.

IV. DATA ANALYSIS TECHNIQUE, CALIBRATION, AND NOISE EQUIVALENT POWER

In order to determine the incident radiated power density distribution on the foil, the technique described in Ref. 11 is used. Before applying this analysis several steps are taken. First of all, the IR images are compensated to eliminate the effects of reflections of nonthermal objects (such as the IR camera cooling element) and variations in the blackbody emissivity of the foil and frame. This is done by subtracting off a reference image which is taken before the discharge begins. Second, the images are reduced from 136×272 pixels to that portion of the image which contains the foil and part of the surrounding frame which consists of 120×160 pixels. Next, the image is resampled using a linear interpolation technique to reduce the image to 12×16 bolometer pixels. This is the equivalent of averaging over 100 IR camera pixels for each bolometer pixel, which reduces the noise in the temperature measurement by a factor of 10. This image consists of a one bolometer pixel border viewing the frame and a 10×14 bolometer pixel view of the foil. Using this data the calculation of the incident radiated power distribution, $P_{\mathrm{rad}}(x,y,t)$, given by Eq. (8) in Ref. 11 is made. This equation is derived using a solution to the two-dimensional heat diffusion equation to solve for the diffusion contribution to the temperature change of the foil. It is rewritten below by separating it into the time derivative term, $P_t(x,y,t)$, and the spatial derivative term, $P_s(x,y,t)$:

$$P_{\mathrm{rad}}(x,y,t)=P_t(x,y,t)+P_s(x,y,t), \tag{1}$$

$$P_t(x,y,t)=t_f k l^2[T(x,y,t)-T(x,y,t-\Delta t)]/\kappa\Delta t, \tag{2}$$

$$P_s(x,y,t)=t_f k[4T(x,y)-T(x,y+l)-T(x,y-l)-T(x+l,y)-T(x-l,y)]_{t-\Delta t}, \tag{3}$$

where $l=6.3$ mm is the dimension of the bolometer pixel, $t_f=1$ μm is the thickness of the foil, $\Delta t=67$ ms is the time between IR camera frames (time resolution), κ is the effective thermal diffusivity of the foil, and k is the effective thermal conductivity of the foil. The effective thermal conductivity and the effective thermal diffusivity are determined through calibration.

Calibration of the IRVB was carried out *in situ* using a 10 mW HeNe laser to heat the foil from the IR camera side using a set of small relay mirrors. The laser beam was aimed at the center of the foil and chopped with a shutter. The beam width of the laser is about 1 mm. By performing the earlier analysis on the resulting data and summing up over the bolometer pixels including and surrounding the beam the absorbed power as a function of time was calculated including the time derivative term and the spatial derivative term. The thermal diffusivity and the thermal conductivity were adjusted to fit the resulting measured power to the laser beam signal as shown in Fig. 4. One notes from this figure that the time derivative term dominates initially, then gives way to the spatial derivative or diffusive term as the foil reaches thermal equilibrium. When the laser power is turned off the time derivative term becomes negative as the foil temperature decays, balancing the diffusive term. The matching o the calculated power to the laser curve required a thermal conductivity that was 3.5 times the value for gold ($k_{\mathrm{AU}}=3.16$ W/cm C) and a thermal diffusivity that was 0.83 times the value for gold ($\kappa_{\mathrm{AU}}=1.27$ cm^2/s). Using the chopped HeNe laser we also observed a variation in the decay time as a function of the distance from the frame. This dependence was modeled as

$$\kappa(x,y)=\kappa[\cos(\pi x/a_x)\cos(\pi y/a_y)]^{0.4}, \tag{4}$$

where a_x and a_y are the dimensions of the foil and x and y are the distances from the center of the foil. Using these calibration factors data from a LHD discharge is analyzed in Sec. V.

An expression for the noise equivalent power for the IRVB derived as Eq. (21) in Ref. 11 is rewritten as the noise equivalent power density (NEPD) by dividing by the bolometer pixel area

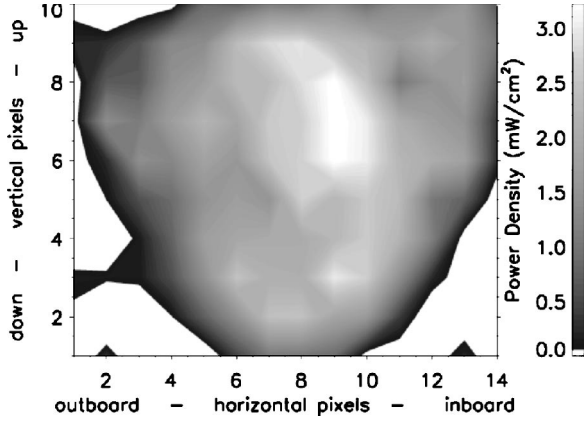

FIG. 5. Image from the IRVB during a discharge using the inboard wall as a limiter.

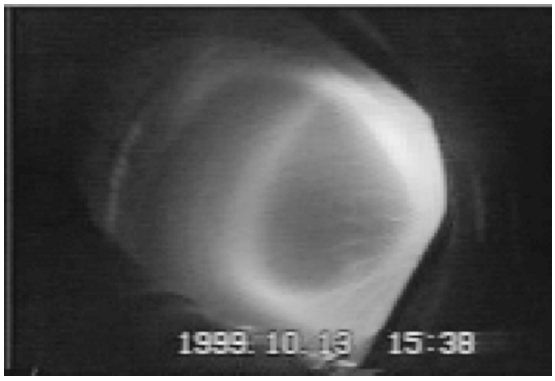

FIG. 6. Image from a CCD camera with H-α filter corresponding to Fig. 5.

$$\eta_{\mathrm{IRVB}}/l^2 = 2\sqrt{2}kt_f \frac{\sigma_{\mathrm{IR}}}{l^2\sqrt{N_{\mathrm{IR}}}}\left(\frac{1}{2}\frac{l^2}{2\kappa\Delta t}+1\right), \tag{5}$$

where σ_{IR} is the IR camera temperature sensitivity and $N_{\mathrm{IR}} = 100$ is the number of IR camera pixels making up one bolometer pixel. The nominal value of σ_{IR} is 80 mK, however, we measure and actual value of 190 mK, which we use for the NEPD calculation. When we include the values for k and κ that we determined from the calibration we get a NEPD of 0.5 mW/cm^2 for this diagnostic when operated in 10×14 pixel mode at 15 Hz.

V. MEASUREMENTS DURING THE LHD EXPERIMENT

In order to demonstrate the usefulness of this diagnostic an image taken from a discharge made in the LHD during the 1999 experimental campaign is shown in Fig. 5. This image comes from a series of discharges where the plasma was scraped off on the inboard vacuum vessel wall. This resulted in a radiation pattern that was localized near the inboard wall as can be seen in the image from the IRVB in Fig. 5 and the image from the charge coupled device (CCD) camera with an H-α filter as seen in Fig. 6. The grid shown in Fig. 3 divides up the view into pixels corresponding to the bolometer pixels indicated by the axis in Fig. 5. The CCD camera is located at the same port but on a flange that is slightly above and to the right of the IRVB, therefore it has a slightly different view. The limit of the field of view of the IRVB as determined by the vacuum vessel wall and other structural components is well defined in the image by a zero level for the power density.

VI. DISCUSSION

The difference in the thermal conductivity derived from the calibration from the actual value for gold may be due to the graphite coating applied to the foil. This may be effectively increasing the thickness of the foil and reducing the sensitivity of the diagnostic without significantly affecting the diffusivity. The possibility of variation in the sensitivity across the foil due to nonuniformities in the foil and nonuniformity in the thickness of the applied graphite layer should be taken into account in the future by calibrating each section of the foil (corresponding to each IR camera pixel as is described in Ref. 11).

ACKNOWLEDGMENTS

The authors are deeply indebted to the LHD team for performing the experiments and to Professor Sudo and Director General Fujiwara for their constant support and encouragement.

[1] G. Miller, J. C. Ingraham, and L. S. Schrank, Rev. Sci. Instrum. **53**, 1410 (1982).
[2] K. F. Mast, J. C. Vallet, C. Adelfinger, P. Betzler, H. Kraus, and G. Schramm, Rev. Sci. Instrum. **62**, 744 (1991).
[3] A. W. Leonard, W. H. Meyer, B. Geer, D. M. Behne, and D. N. Hill, Rev. Sci. Instrum. **66**, 1201 (1995).
[4] TFR Group (presented by A. L. Pecquet), J. Nucl. Mater. **93–94**, 377 (1980).
[5] J. C. Ingraham and G. Miller, Rev. Sci. Instrum. **54**, 673 (1983).
[6] G. Apruzzese and G. Tonini, Rev. Sci. Instrum. **61**, 2976 (1990).
[7] G. A. Wurden, in *Diagnostics for Experimental Thermonuclear Fusion Reactors*, edited by P. E. Stott *et al.* (Plenum, New York, 1996), pp. 603–606.
[8] G. A. Wurden, B. J. Peterson, and S. Sudo, Rev. Sci. Instrum. **68**, 766 (1997).
[9] G. A. Wurden and B. J. Peterson, Rev. Sci. Instrum. **70**, 255 (1999).
[10] N. Ashikawa, B. J. Peterson, G. A. Wurden, and S. Sudo, J. Plasma Fusion Res. (to be published).
[11] B. J. Peterson, Rev. Sci. Instrum. **71**, 3696 (2000).
[12] B. J. Peterson, S. Sudo, and the CHS Group, J. Plasma Fusion Res. **1**, 382 (1998).